

Probing signatures of fractionalisation in candidate quantum spin liquid Cu_2IrO_3 via anomalous Raman scattering

Srishti Pal,¹ Arnab Seth,² Piyush Sakrikar,³ Anzar Ali,³ Subhro Bhattacharjee,² D. V. S. Muthu,¹ Yogesh Singh,³ and A. K. Sood^{1,*}

¹*Department of Physics, Indian Institute of Science, Bengaluru 560012, India*

²*International Centre for Theoretical Sciences,*

Tata Institute of Fundamental Research, Bengaluru 560089, India

³*Indian Institute of Science Education and Research (IISER) Mohali,*

Knowledge City, Sector 81, Mohali 140306, India

Abstract

Long-range entanglement in quantum spin liquids (QSLs) lead to novel low energy excitations with fractionalised quantum numbers and (in 2D) statistics. Experimental detection and manipulation of these excitations present a challenge particularly in view of diverse candidate magnets. A promising probe of fractionalisation is their coupling to phonons. Here we present Raman scattering results for the $S = 1/2$ honeycomb iridate Cu_2IrO_3 , a candidate Kitaev QSL with fractionalised Majorana fermions and Ising flux excitations. We observe anomalous low temperature frequency shift and linewidth broadening of the Raman intensities in addition to a broad magnetic continuum both of which, we derive, are naturally attributed to the phonon decaying into itinerant Majoranas. The dynamic Raman susceptibility marks a crossover from the QSL to a thermal paramagnet at ~ 120 K. The phonon anomalies below this temperature demonstrate a strong phonon-Majorana coupling. These results provide for evidence of spin fractionalisation in Cu_2IrO_3 .

* E-mail: asood@iisc.ac.in

Recent advances in condensed matter physics and material sciences have shown that several so-called *elementary particles*, originally conceived in context of high energy physics can emerge as low energy excitations (quasi-particles) in condensed matter systems. In addition to providing an impetus to the paradigm of emergent quantum phenomena [1–3], these materials then provide concrete contexts to understand the properties of these novel excitations and the settings for their emergence as an interplay of symmetries and many-body entanglement. This ranges from the weakly correlated physics of Dirac fermions in monolayer graphene [4, 5] and Weyl fermions in topological semimetals [6–8] on one hand to the strongly correlated fractionalised excitations in fractional quantum Hall systems [9, 10].

In this context, the possibility of emergence of the elusive (in high energy particle physics) Majorana fermion [11, 12] in several candidate solid state systems like topological superconductors [13–17], fractional quantum Hall systems [18], and QSLs [19–22] have been invoked to account for startling novel low energy properties of these systems. Among them, the Kitaev QSL [19] on isotropic honeycomb lattice provides a unique opportunity where propagating Majorana excitations coupled to emergent Z_2 fluxes arise due to the long-range quantum entanglement present in the system resulting in the fractionalisation of the underlying microscopic spin-1/2s [19].

Our present understanding suggests that a key ingredient in realising Kitaev physics is specific *compass* spin-spin interactions [23, 24] on a tri-coordinated motif consisting of edge-sharing octahedra [23, 25]. Our growing understanding of magnets with strong spin-orbit coupling have provided a slew of such candidate Kitaev QSL materials containing 4d and 5d transition metal ions. The most notable ones among these are Na_2IrO_3 [26] and $\alpha\text{-RuCl}_3$ [27] on two-dimensional layered honeycomb motif and γ - and $\beta\text{-Li}_2\text{IrO}_3$ [28] on three-dimensional hyper-honeycomb lattice. A combination of thermodynamic measurements and scattering experiments [21, 29] on these “first-generation” Kitaev materials show extremely interesting finite temperature behaviour including possible signatures of fractionalisation and thereby raise questions about their proximity to a Kitaev (or other) QSLs [20, 21, 30]. However, they ultimately order magnetically at a much lower temperature possibly due to additional non-Kitaev interactions in these systems. Thus, while the above compounds are very interesting in their own rights to understand the possible interplay of magnetic fluctuations and fractionalisation, the realisation of the Kitaev QSL with pristine signatures of the fractionalised Majoranas still remains an open issue.

In this paper, we report our results on the Raman scattering and magneto-elastic coupling of the “second-generation” Kitaev material, Cu_2IrO_3 [31], where the magnetic order is absent suggesting the possibility of smaller non-Kitaev interactions. In particular, despite a Curie-Weiss temperature and effective magnetic moment similar to Na_2IrO_3 , μSR and specific heat studies on Cu_2IrO_3 have shown an absence of magnetic order and an excitation spectrum dominated by low-energy Ir spin dynamics [32, 33]. The correlated nature of this low temperature paramagnet is further supported by the NQR measurements [34]. These findings suggest that Cu_2IrO_3 may offer an ideal playground to investigate fractionalisation in a Kitaev QSL with an eye towards positive characterisation of the Majorana fermions therein. An additional topic of current interest, which has not been explored in experiments yet, is the Majorana-optical phonon coupling which has only been studied theoretically so far for the acoustic phonons in the Kitaev model [35–37].

Strong spin-orbit coupling results in intricate mixing of the real and spin space. Thus, on generic grounds one expects these compounds to have enhanced spin-lattice coupling. Can this spin-(optical) phonon coupling, as probed in Raman scattering, then lead to positive identification of the possible fractionalised excitations (Majorana fermions in a Kitaev QSL) in candidate QSL materials such as Cu_2IrO_3 ? The central result of our work is the anomalous shift and broadening of the Raman active phonons in Cu_2IrO_3 (Fig. 2) which indicate extra decay channels become active at low temperatures for the low energy Raman active phonons. In absence of magnetic order, a natural candidate for coherent modes that can result in phonon decay, within Kitaev phenomenology, are itinerant Majorana fermions. Indeed, we find that such fractionalisation do provide a successful explanation for our Raman measurements. Our estimate of the Kitaev exchange from the band edge of the magnetic continuum is consistent with earlier NQR measurements. The temperature dependence of Raman susceptibility is non-monotonic and clearly evidences fermionic Majorana excitations prevailing over a conventional Bosonic background below about 120 K.

The “second-generation” Kitaev materials, such as Cu_2IrO_3 , are obtained by partially or fully replacing the alkali atoms in $\alpha\text{-A}_2\text{IrO}_3$ with other atoms. Incredibly, the new materials produced in this manner, $\text{H}_3\text{LiIr}_2\text{O}_6$ [38], Cu_2IrO_3 [31], and $\text{Ag}_3\text{LiIr}_2\text{O}_6$ [39], have been shown to be QSL candidates with no signatures of magnetic order using various thermodynamic and dynamic probes [32, 34, 38, 39]. In these second generation Kitaev materials, the edge-sharing IrO_6 octahedra forming a honeycomb lattice plane is retained. However, the

interplanar connectivity is changed. For example, Cu_2IrO_3 crystallises in the same $C2/c$ monoclinic structure as Na_2IrO_3 . The honeycomb layers are formed by an edge-sharing $(\text{Ir}_{2/3}\text{Cu}_{1/3})\text{O}_6$ octahedral arrangement identical to Na_2IrO_3 , but the interlayer connections via distorted NaO_6 octahedra are replaced by linear CuO_2 dumbbells resulting in a larger c -axis. This enhanced 2D character of the honeycomb layers along with the proximity of the Ir-Ir-Ir angles towards the ideal value of 120° compared to its predecessor Na_2IrO_3 , puts copper iridate closer to the ideal Kitaev limit. Similar interlayer bonding is found for $\text{H}_3\text{LiIr}_2\text{O}_6$ [38] and $\text{Ag}_3\text{LiIr}_2\text{O}_6$ [39].

The nature of the synthesis makes these second generation Kitaev materials prone to disorder. For example, proton positional disorder in $\text{H}_3\text{LiIr}_2\text{O}_6$, or Cu and Ir site disorder in Cu_2IrO_3 . The possible role of disorder in stabilising the QSL in these materials has been discussed recently [32, 38, 40–42]. In the context of Raman measurements, the proton disorder in $\text{H}_3\text{LiIr}_2\text{O}_6$ has been suggested to lead to the observed anomalously broad phonon modes as well as the weak fermionic contribution to the magnetic continuum [43]. For Cu_2IrO_3 as well, the disorder can lead to measurable consequences. Initial reports observed a glassy state at low temperatures using magnetic susceptibility [31]. μSR measurements on these samples showed that a significant fraction of the magnetic moments indeed freeze at low temperatures [33]. We have been able to synthesise high quality Cu_2IrO_3 samples which do not show any features of a glassy state either in ac magnetic susceptibility [44] or in μSR down to 260 mK [32].

We have therefore chosen the second generation Kitaev material Cu_2IrO_3 to study the fractionalisation predicted in the Kitaev model [45]. Neutron scattering on iridates is difficult because of the strong absorption of neutrons by iridium, although some efforts to measure iridates using special experimental setups have been reported [46]. Probing the phonons via inelastic light scattering can reveal the fate of the magnetic degrees of freedom via spin-lattice coupling. This can be particularly strong in spin-orbit coupled compounds due to the non-trivial nature of the $J = 1/2$ spins coupling the real and the spin-space. Indeed, in Raman scattering for γ - and β - Li_2IrO_3 [28], α - RuCl_3 [47–49] and $\text{H}_3\text{LiIr}_2\text{O}_6$ [43], a broad magnetic continuum has been detected in the low-energy Raman profile. Even though γ - and β - Li_2IrO_3 and α - RuCl_3 have magnetically ordered ground states, the temperature evolution of the magnetic background is typified by dominant Fermi statistics and has been attributed

to the fractionalised Majorana fermions [28, 47–49].

Experimental Results

Fig. 1(a) shows unpolarised Raman spectra of Cu_2IrO_3 at a few representative temperatures with sharp phonon modes superimposed on a broad continuum extending up to $\sim 600 \text{ cm}^{-1}$. As observed experimentally in other Kitaev materials $\alpha\text{-RuCl}_3$ [47–49] and $\gamma\text{-}$ and $\beta\text{-Li}_2\text{IrO}_3$ [28], phonons are superimposed on a broad background which is temperature dependent. This broad Raman background in experiments has been attributed to the gapless itinerant Majorana fermions of a Kitaev QSL. Finite temperature simulations for the Kitaev model by Nasu et al. [50] reproduce the broad continuum with a band edge extending up to $\simeq 3 |J_K|$ (arising from the Majorana fermion bandwidth) where J_K is the Kitaev coupling strength. As shown in Fig. 1, the upper cut-off of the magnetic continuum in Cu_2IrO_3 gives an experimental estimate for $|J_K| \approx 24 \text{ meV}$, in good agreement with recent estimates (17 to 30 meV) from the low-energy spin excitation gap seen in NQR studies [34]. This intriguing broad magnetic continuum (Fig. 1) then begs for a careful closer investigation - a topic to which we shall now focus on.

Anomalies in frequencies and linewidths of Raman active phonons : Apart from signatures consistent with fractionalisation into Majorana fermions, we now look for the effect of Majorana excitations on phonons, if any, especially at low temperatures ($T \lesssim J_K$). Of the 39 active Raman modes expected for monoclinic ($C2/c$) Cu_2IrO_3 ($\Gamma_{\text{Raman}} = 18A_g + 21B_g$), 13 modes could be detected at $\sim 6 \text{ K}$ in the frequency range $70\text{-}800 \text{ cm}^{-1}$ (8.7 - 99.2 meV). All the phonon modes are fitted with symmetric Lorentzian profile function for the entire range of temperature. The overall phonon spectrum remains almost unchanged with increasing temperature except for the thermal broadening of weaker modes making them undetectable at higher temperatures. No change in the number of Raman modes confirm the stability of the ambient crystal symmetry down to 6 K. This is an advantage that Cu_2IrO_3 has over $\alpha\text{-RuCl}_3$, which undergoes a structural transition around 140 K, further obscuring attempts to establish connections between the onset of Majorana fermions and phonons [49].

Normally, a monotonic temperature dependence of phonon parameters is expected because the phonon self-energies are typically determined by lattice anharmonicity which reduces monotonically with temperature [51]. This is however not the case in Cu_2IrO_3 with anomalous temperature evolution of frequencies and FWHMs of the phonon modes below

$T \simeq 120$ K. The temperature dependence of the frequency and FWHMs of the strong phonon modes (marked M1, M2, M3 and M4 in Fig. 1 and Fig. S4(a)) are shown in Fig. 2(a)-(b). The solid blue lines are linear fits between 295 K and 120 K to the approximated simple cubic anharmonic model [52] as, $\omega = \omega_0 + AT$ and $\Gamma = \Gamma_0 + BT$ where, ω_0 and Γ_0 are frequencies and linewidths at absolute zero, A (negative) and B (positive) are anharmonic constants. The dashed lines are extrapolations of the fits to lower temperatures. The frequencies (FWHM) are lower (higher) than expectation from the cubic anharmonic temperature dependence of phonons. This effect though most dramatic for M1 is seen for all modes below $T \lesssim 120$ K $\approx 0.43 J_K$. The above anomaly is very much different from the phonon softening in magnetically ordered materials, such as Fe_3GeTe_2 [53], where similar anomalies are associated with the magnetic order. For Cu_2IrO_3 , however, no such magnetic order is present down to the lowest temperature measured.

Remarkably, the numerical studies [50, 54] of the pure Kitaev model found that such a temperature scale, $T_h \sim 0.4-0.5 J_K$, is associated with the completion of transfer of spectral weight of a coherent itinerant Majorana fermion to an incoherent one. Indeed, the above temperature is associated with the van-Hove singularity of the free Majorana dispersion in the zero-flux sector whose depletion is completed at $T \sim T_h$. The above agreement of T_h with that of the pure Kitaev model numerics is seen for all the Raman-active modes. At this point, we note that for the Kitaev QSL there is another energy-scale $T_l \sim 0.012-0.015 J_K$ associated with the Z_2 fluxes [19, 50, 54]. Although such low temperature is not accessible to the current experiment, the frequency (FWHM) of the phonon decreases(increases) monotonically till the lowest accessible temperature, $T \sim 6.5$ K.

Intensity of M3 mode : In absence of spin-lattice coupling, the temperature dependence of integrated intensities of Raman phonons should follow the conventional Bose-Einstein distribution. The high-frequency M3 mode ($\hbar\omega_{M3} \approx 63$ meV) shows a strong departure from the above expectation and shows a strong enhancement of intensity with decreasing temperatures as seen in Fig. 1. In fact, we find (see SI [44]) that the intensity of M3 closely follows the temperature dependence of the DC susceptibility and thus dependent on the spin-spin correlation. The susceptibility, in turn, shows clear deviation from the high-temperature Curie-Weiss (CW) behaviour below ~ 120 K. Such anomalous behaviour can arise from transfer of magnetic dipole spectral weight to the phonons via spin-lattice coupling [55]. Indeed, the phonon intensities are expected to depend on the

spin-spin correlations [56]. This reiterates the presence of sizeable spin-lattice coupling in Cu_2IrO_3 .

Low-energy magnetic continuum : Within the Kitaev QSL phenomenology, which presently forms the natural framework to understand the anomalous spin-phonon coupling, we attribute the low energy magnetic continuum to that of the Majorana fermions scattering from the Z_2 fluxes. In particular the effect of the low energy Z_2 fluxes on the Majorana fermions inside the QSL is to renormalise the fermion bandwidth and density of states [50, 54]. In order to extract Majorana fermionic energy scale from the low-energy continuum, following [50], the Raman intensity $I(\omega)$ is integrated over the intermediate frequency range of $\omega_{min} < \omega < \omega_{max}$ to obtain $I_{mid} = \int_{\omega_{min}}^{\omega_{max}} I(\omega)d\omega$. The temperature dependence of I_{mid} in the frequency interval 90 to 230 cm^{-1} is plotted in the inset of Fig. 3. As is clear from the inset, I_{mid} has a non-monotonic temperature dependence with the high temperature regime dominated by the standard one-particle scattering due to thermal Bose factor $[1 + n(\omega_b)] = 1/(1 - e^{-\hbar\omega_b/k_B T})$, with $\omega_b = 11$ meV, extracted from the Bosonic fit as a fitting parameter. This Bosonic background is attributed to phonons since the system does not entertain other Bosonic excitations like magnons due to lack of long-range spin ordering down to lowest measurable temperature. A confirmation of this is obtained from the fact that the value of ω_b matches well with the strongest phonon mode at 92 cm^{-1} in the low-frequency regime.

The main panel of Fig. 3 demonstrates the temperature evolution of integrated I_{mid} after subtracting the non-magnetic Bosonic background. The magnetic contribution to I_{mid} enhances significantly below 120 K as clearly indicated by deviation from thermal behaviour and can be well fitted to the form [50] $A + B[1 - f(\omega_f)]^2$ with $\omega_f = 18$ meV, where $f(\omega_f) = 1/(1 + e^{\hbar\omega_f/k_B T})$ is the Fermi distribution function. This typical scaling of I_{mid} is associated with the scattering contribution from the process of creation or annihilation of Majorana fermion pairs [50]. The Majorana energy scale for Cu_2IrO_3 is deduced from the fermionic fit with $\omega_f = 18$ meV ($\approx 0.8|J_K|$) and is in accordance with a Kitaev QSL phase considering similar energy scales gleaned for other Kitaev candidates [28, 50].

To further extract the Majorana essence from the magnetic background, dynamic spin susceptibility χ_R is measured. The magnetic Raman susceptibility χ_R is extracted by integrating Raman conductivity $\frac{\chi''(\omega)}{\omega}$ in the frequency range 70 to 600 cm^{-1} using Kramers-Kronig relation, $\chi_R = \lim_{\omega \rightarrow 0} \chi(k = 0, \omega) \equiv \frac{2}{\pi} \int \frac{\chi''(\omega)}{\omega} d\omega$. The dynamical Raman tensor susceptibility $\chi''(\omega)$ is proportional to Raman intensity as $I(\omega) = 2\pi \int \langle R(t)R(0) \rangle$

$e^{i\omega t} dt \propto [1 + n(\omega)]\chi''(\omega)$, where $R(t)$ is the Raman operator. Fig. 4 displays the temperature dependence of χ_R which shows that it remains almost constant down to 120 K, below which it increases rapidly with decreasing temperature. In the Kitaev QSL state, the Raman operator couples to the dispersing Majorana fermions and extensively projects to the two-Majorana fermion density of states (DOS) [57]. Thus, an enhancement of χ_R below 120 K corresponds to significant enhancement of Majorana DOS in the system driving the system from a simple paramagnet to a Kitaev paramagnet, also clearly reflected in temperature dependence of I_{mid} .

Both I_{mid} in Fig. 3 and χ_R in Fig. 4 show a subtle decrease below ~ 25 K. At a first glance, one may correlate this with the partial spin-freezing reported for Cu_2IrO_3 below ~ 10 K in recent μSR and NQR studies [33, 34]. However, this may not be the case as our samples do not show evidence of spin-freezing down to 2 K in ac χ [44] as well as down to 260 mK in μSR measurements [32]. It is tempting to associate the decrease in I_{mid} below 25 K ($\sim 0.09J_K$) to the calculated I_{mid} by quantum Monte Carlo calculations (peaking at $\sim 0.07J_K$) [50].

Majorana-phonon coupling

In absence of any thermal phase transition to a magnetic ordered state, the anomalous renormalisation of the phonon frequency and increment in the linewidth at low temperatures suggest that new decay channels are opening up for the phonons to interact and possibly decay into. Given the current understanding of the phenomenology of Cu_2IrO_3 [32–34] and the encouraging match of the the energy-scale T_h , it is natural to seek an explanation of the above experiments in terms of the excitations of the Kitaev QSL, *i.e.* the Majorana fermions and Z_2 fluxes. Already, the existing calculations [50, 54] correctly accounts for the broad magnetic background in Fig. 1 to this end.

We now show that the spin-phonon coupling leads to the possibility of a Yukawa-like coupling between a Majorana bilinear and the phonon somewhat akin to the electron-phonon coupling in superconductivity (in the present case, however there is no charge conservation). This coupling, in turn, accounts for the experimental findings and hence provides a very interesting understanding of the experimental data in terms of the Majorana-phonon coupling. Below, we outline our calculations capturing the essence of the above physics. The Kitaev spin model is given by [19]

$$H_{\text{Kitaev}} = \sum_{i,\alpha} J_{i,\alpha} S_i^\alpha S_{i+\hat{\alpha}}^\alpha \quad (1)$$

where α denotes x, y or z type of bonds and $\hat{\alpha}$ denotes the three nearest neighbour vectors of honeycomb lattice. The exchange couplings are functions of the ionic positions as they come from the overlap of the electronic wave-functions. Thus, in presence of Lattice vibrations, we have [58]

$$J_{i,\alpha} = J_K + \frac{\partial J_{i,\alpha}}{\partial R_{i,\alpha}^a} \delta_{i,\alpha}^a + \frac{1}{2} \frac{\partial^2 J_{i,\alpha}}{\partial R_{i,\alpha}^a \partial R_{i,\alpha}^b} \delta_{i,\alpha}^a \delta_{i,\alpha}^b \quad (2)$$

where the expansion is done about the equilibrium ionic positions of the crystal, $\bar{R}_{i,\alpha}^a = r_i^a - r_{i+\hat{\alpha}}^a$ with $\delta_{i,\alpha}^a = R_{i,\alpha}^a - \bar{R}_{i,\alpha}^a$ ($a = x, y$) denoting the deformation of the bond and the derivatives are evaluated at the equilibrium position \bar{R}_{ij} .

This leads to the spin-phonon Hamiltonian that dictates the coupled dynamics of the optical phonons and the spins

$$H = H_{\text{spin}} + H_{\text{spin-phonon}} + H_{\text{phonon}} \quad (3)$$

where H_{spin} is the bare spin Kitaev Hamiltonian of Eq. 1 with $J_{i,\alpha} \rightarrow J_K$, H_{phonon} is the bare Harmonic phonon Hamiltonian and

$$H_{\text{spin-phonon}} = H_1 + H_2 \quad (4)$$

represents the spin-phonon coupling. The two terms denote the first and second order contributions of Eq. 2 and are given by

$$H_1 = \sum_{i,\alpha} \frac{\partial J_{i,\alpha}}{\partial R_{i,\alpha}^a} \delta_{i,\alpha}^a S_i^\alpha S_{i+\hat{\alpha}}^\alpha \quad (5)$$

and

$$H_2 = \frac{1}{2} \sum_{i,\alpha} \frac{\partial^2 J_{i,\alpha}}{\partial R_{i,\alpha}^a \partial R_{i,\alpha}^b} \delta_{i,\alpha}^a \delta_{i,\alpha}^b S_i^\alpha S_{i+\hat{\alpha}}^\alpha \quad (6)$$

respectively. Expressing the phonons in terms of their normal modes and neglecting the various form factors which we expect to be unimportant for the generic temperature dependence that we are focussing on, we now obtain the renormalisation of the phonon frequency and linewidth by calculating the self-energy correction to the phonon propagators due to the above spin-phonon interactions within a single mode approximation for the phonons.

Within the Kitaev QSL phenomenology, we perform the standard Majorana decoupling of the spins to obtain (in the zero-flux sector) the scattering vertices between the matter fermions and the phonons as shown in Fig. 5. Here we have performed the well-known [59] transformation of the Majoranas to the bond matter fermions for the Kitaev QSL. Also, the upper and lower panels denote the interaction vertices arising due to H_1 (Eq. 5) and H_2 (Eq. 6), respectively.

These interactions clearly show that the phonon can decay into the fractionalised excitations of the QSL and this would renormalise both the frequency and the linewidth of the phonon peak. In regard to the linewidth, we expect that an anomalous broadening as the temperature is decreased since on lowering the temperature the fermions become more coherent and hence the phonon can more efficiently decay into them while obeying all the conservation laws.

Frequency renormalisation : The leading order contribution to the renormalisation of the frequency comes from the lower panel of Fig. 5 when we integrate over the fermions. From Eq. 5, the resultant frequency renormalisation is given by

$$\delta\omega \propto \frac{1}{N_b} \sum_{i,\alpha} \langle \bar{J}_K S_i^\alpha S_{i+\hat{\alpha}}^\alpha \rangle_S \quad (7)$$

where $\langle \dots \rangle_S$ denotes averaging of the equal time spin correlators over the thermodynamic ensemble and the proportionality constant is given in terms of the first order spin-phonon coupling and the transformation to the phonon soft modes. For the present discussion we neglect their detail structure and assume it to be a constant, λ .

Within a free Majorana phenomenology the spin-energy can be calculated in the zero-flux sector to obtain and estimate of $\delta\omega$. This calculation is detailed in SI [44] and it readily matches the expectation that it goes to zero at $T \rightarrow \infty$ and gradually turns non-zero around $T \sim J_K$ ultimately saturating to a negative constant number at zero temperature corresponding to the ground state energy-density of the spins. Further, numerical calculations exist for

finite temperatures including all the flux sectors for the pure Kitaev model [54] which shows that a rather sharp crossover from zero to non-zero values. With the energy being generally negative this nominally suggests softening of the phonon frequency. We however note that the mode dependence of the above contribution is entirely due to the matrix elements which we have neglected in this calculation. Further temperature dependence can come from the real part of the self-energy of the bubble (see SI [44] for details).

Phonon Linewidth : The leading contribution to the line-width, however comes from the bubble contributions arising due to the two vertices in the lower panel of Fig. 5. At finite temperature and in presence of spin-interactions beyond the pure Kitaev model, clearly the fermion lines would be further renormalised by its scattering with the Z_2 fluxes, which, in turn, provide finite lifetime to the fermions as well as renormalise their bandwidth [19]. For very low temperature and within the exactly solvable model, we neglect the scattering with the gapped Z_2 fluxes and then we have free Majorana fermions which seems to be justified on the basis of the numerical calculations [50, 54] which shows that the qualitative features of the matter fermion density of states remain intact at finite temperatures almost all the way up to T_h . Within this free Majorana phenomenology, we now calculate the leading order contribution to the Raman linewidth computing the self-energy bubble diagram for a particular normal mode. The imaginary part of the phonon self-energy correction at the leading order is then given by

$$Im[\Sigma(\mathbf{q}, \omega + i0^+)] \propto \frac{J_K^2}{N_b} \sum_{\mathbf{k}} (1 - n_F(\epsilon_{\mathbf{k}}) - n_F(\epsilon_{\mathbf{k}+\mathbf{q}})) \left[\delta(\omega + \epsilon_{\mathbf{k}} + \epsilon_{\mathbf{k}+\mathbf{q}}) - \delta(\omega - \epsilon_{\mathbf{k}} - \epsilon_{\mathbf{k}+\mathbf{q}}) \right] \quad (8)$$

where, again, the proportionality constant depends on the magneto-elastic coupling and the normal-mode matrix elements which have been assumed to be a constant(χ) for this calculation. Here $n_F(\epsilon_{\mathbf{k}})$ denotes the fermion occupancy of the complex fermionic modes with dispersion $\epsilon_{\mathbf{k}}$ in the zero-flux sector. This contribution, as the delta function indicates, arises due to the decay of the phonon into two fermions. As $T \rightarrow \infty$, the Majorana fermions become incoherent and hence the above contribution to linewidth goes to zero, while at low temperatures it reaches a finite value for the completely coherent Majorana fermions.

This effect is completely opposite of the usual temperature related broadening due to anharmonic terms and arises due to the development of a coherent scattering channel for

the phonons. Clearly, in absence of any magnetic phase transition, such coherent particles - in case of a Kitaev QSL Majorana fermions - indicate novel low temperature physics in the spin sector. This is in direct conformity with the experimental observation. Once the flux excitation is taken into account, it only renormalises the free Majorana contribution without changing its qualitative features. We note that the real part of the self-energy coming from the bubble further renormalises the phonon frequency and hence contributes to $\delta\omega$ in Eq. 7. Here we neglect such higher order contributions.

The phonon intensity obtained from the above calculation is given by the Lorentzian form

$$\frac{4\omega_0^2 \text{Im}[\Sigma]}{(\omega^2 - \omega_0^2 - 2\omega_0\delta\omega)^2 + 4\omega_0^2 \text{Im}[\Sigma]^2} \quad (9)$$

where ω_0 is the bare phonon frequency of a particular normal mode. We evaluate the above expression considering $q \rightarrow 0$ limit (which is relevant to the experiment) in Eq 8.

We plot the Stokes line in Fig. 6. This is in qualitative agreement with the experimental data. A further comparison with the experimental data is obtained by fitting the results to the experimental data as shown in SI [44].

To account for the temperature dependence of intensity for the $M3$ mode, we note that the intensity is generically of the form [56] $|A + B_\alpha \langle S_i^\alpha S_{i+\hat{\alpha}}^\alpha \rangle|^2$, *i.e.* proportional to the nearest neighbour spin correlations. This, within free Majorana fermions can be calculated to yield a dependence proportional to $|\delta\omega|$ as is clear from Eq. 1. While such effects should appear for all the four modes, the particular sensitivity of $M3$ appears to us as a matrix-element effect that requires further calculations.

Summary and Outlook

To summarise, we have investigated the Raman response of the “second-generation” Kitaev QSL candidate Cu_2IrO_3 . In addition to the the magnetic continuum (consistent with the Kitaev coupling, $J_K \approx 24$ meV) observed in the “first-generation” Kitaev materials, we observe clear anomalous renormalisation of the Raman-active phonons below ~ 120 K. Encouraged by the conformity of the energy-scales of the magnetic continuum and the phonon anomaly within a Kitaev phenomenology, we investigate the qualitative features of the Majorana-(optical) phonon coupling to make an estimate for the phonon anomaly which accounts for the experimental observations.

Our results thus provide strong indication for the relevance of Kitaev QSL physics and the immensely exciting possibility of positive identification of fractionalisation in the nearly perfect honeycomb iridate Cu_2IrO_3 . This opens several interesting questions from both experimental and theoretical sides. On the experimental front, several future directions of study can be envisaged. Single crystals of Cu_2IrO_3 are not currently available. With single crystals, polarisation dependent Raman studies will become possible which will allow a further quantitative comparison between theoretical calculations and experiments to further substantiate the physics of Majorana-phonon coupling. Additionally, inelastic neutron scattering to measure the energy and momentum dependent excitation spectrum are desirable to be able to make quantitative comparisons with specific Hamiltonians including the Kitaev model and its extensions. Finally, crystals will allow looking for quantisation in thermal Hall measurements, similar to what has been reported for $\alpha\text{-RuCl}_3$ [60]. On the theoretical side, the present calculation only takes care of the free Majorana fermions while neglects the fluxes as well as other non-Kitaev spin interactions. Their roles in the present calculations needs to be quantitatively settled both for Cu_2IrO_3 and other QSLs in general to investigate the physics of fractionalisation through phonons.

Methods

Synthesis and Characterisation : High quality polycrystalline samples of Cu_2IrO_3 were prepared by a low temperature topotactic reaction of Na_2IrO_3 with CuCl as reported previously [32, 44]. Powder X-ray diffraction confirmed the expected crystal structure (C2/c space group) and ac and dc susceptibility measurements down to 300 mK [44] confirmed the absence of spin-freezing which has been reported to contaminate the low temperature magnetism for some Cu_2IrO_3 materials reported previously [31, 34].

Raman Scattering : The unpolarised Raman spectra at room temperature were recorded in a backscattering geometry using Horriba LabRAM HR Evolution Spectrometer equipped with a thermoelectric cooled charge coupled device (CCD) (HORIBA Jobin Yvon, SYNCERITY 1024 X 256). The low temperature Raman measurements were performed from 6 K to 295 K with 532 nm DPSS laser illuminating the sample with less than ~ 1.5 mW power. Temperature variation was done with closed cycle He cryostat (Cryostation

S50, Montana Instruments) with a temperature stability of $\approx \pm 1$ K.

Acknowledgements

AKS thanks Nanomission Council and the Year of Science professorship of DST for financial support. PS, AA and YS thank the X-ray, liquid Helium plant and the SQUID magnetometer facilities at IISER Mohali. SB acknowledges J. Knolle and R. Moessner for previous collaborations and A. Nanda and K. Damle for discussions. SB acknowledge Max Planck Partner Grant at ICTS and SERB-DST (India) project grant No. ECR/2017/000504 for funding. SB and AS acknowledge support of the Department of Atomic Energy, Government of India, under project no.12-R&D-TFR-5.10-1100.

Author Contributions

AKS, SP, DVSM and YS formulated the study. SP carried out Raman measurements and data analysis. Sample preparation along with structural and magnetic characterisations were done by PS and AA in the group of YS. Theoretical calculations were done by AS and SB. All the authors contributed to the manuscript preparation.

-
- [1] P. W. Anderson, *Science* **177**, 393 (1972).
 - [2] R. B. Laughlin and D. Pines, *PNAS* **97**, 28 (2000).
 - [3] X. G. Wen, *Rev. Mod. Phys.* **89**, 041004 (2017).
 - [4] A. H. C. Neto, F. Guinea, N. M. R. Peres, K. S. Novoselov, and A. K. Geim, *Rev. Mod. Phys.* **81**, 109 (2009).
 - [5] K. S. Novoselov, A. K. Geim, S. V. Morozov, D. Jiang, M. I. Katsnelson, I. V. Grigorieva, S. V. Dubonos, and A. A. Firsov, *Nature* **438**, 197 (2005).
 - [6] X. Wan, A. M. Turner, A. Vishwanath, and S. Y. Savrasov, *Phys. Rev. B* **83**, 205101 (2011).
 - [7] B. Yan and C. Felser, *Annu. Rev. Condens. Matter Phys.* **8**, 337 (2017).
 - [8] N. P. Armitage, E. J. Mele, and A. Vishwanath, *Rev. Mod. Phys.* **90**, 015001 (2018).
 - [9] N. Read and D. Green, *Phys. Rev. B* **61**, 10267 (2000).
 - [10] C. Nayak, S. H. Simon, A. Stern, M. Freedman, and S. D. Sarma, *Rev. Mod. Phys.* **80**, 1083 (2008).
 - [11] F. Wilczek, *Nat. Phys.* **5**, 614 (2009).

- [12] J. Alicea, *Rep. Prog. Phys.* **75**, 076501 (2012).
- [13] A. Y. Kitaev, *Physics-Uspekhi* **44**, 131 (2001).
- [14] X. L. Qi and S. C. Zhang, *Rev. Mod. Phys.* **83**, 1057 (2011).
- [15] S. D. Sarma, C. Nayak, and S. Tewari, *Phys. Rev. B* **73**, 220502(R) (2006).
- [16] A. Das, Y. Ronen, Y. Most, Y. Oreg, M. Heiblum, and H. Shtrikman, *Nat. Phys.* **8**, 887 (2012).
- [17] V. Mourik, K. Zuo, S. M. Frolov, S. R. Plissard, E. P. A. M. Bakkers, and L. P. Kouwenhoven, *Science* **336**, 1003 (2012).
- [18] M. Banerjee, M. Heiblum, V. Umansky, D. E. Feldman, Y. Oreg, and A. Stern, *Nature* **559**, 205 (2018).
- [19] A. Kitaev, *Ann. Phys.* **321**, 2 (2006).
- [20] Y. Kasahara, T. Ohnishi, Y. Mizukami, O. Tanaka, S. Ma, K. Sugii, N. Kurita, H. Tanaka, J. Nasu, Y. Motome, T. Shibauchi, and Y. Matsuda, *Nature* **559**, 227 (2018).
- [21] A. Banerjee, C. A. Bridges, J. Q. Yan, A. A. Aczel, L. Li, M. B. Stone, G. E. Granroth, M. D. Lumsden, Y. Yiu, J. Knolle, S. Bhattacharjee, D. L. Kovrizhin, R. Moessner, D. A. Tennant, D. G. Mandrus, and S. E. Nagler, *Nat. Mater.* **15**, 733 (2016).
- [22] G. Chen, A. Essin, and M. Hermele, *Phys. Rev. B* **85**, 094418 (2012).
- [23] G. Jackeli and G. Khaliullin, *Phys. Rev. Lett.* **102**, 017205 (2009).
- [24] Z. Nussinov and J. van den Brink, *Rev. Mod. Phys.* **87**, 1 (2015).
- [25] J. G. Rau, E. K. H. Lee, and H. Y. Kee, *Phys. Rev. Lett.* **112**, 077204 (2014).
- [26] K. Mehlawat, A. Thamizhavel, and Y. Singh, *Phys. Rev. B* **95**, 144406 (2017).
- [27] S. H. Do, S. Y. Park, J. Yoshitake, J. Nasu, Y. Motome, Y. S. Kwon, D. T. Adroja, D. J. Voneshen, K. Kim, T. H. Jang, J. H. Park, K. Y. Choi, and S. Ji, *Nat. Phys.* **13**, 1079 (2017).
- [28] A. Glamazda, P. Lemmens, S. H. Do, Y. S. Choi, and K. Y. Choi, *Nat. Comms.* **7**, 12286 (2016).
- [29] A. Banerjee, J. Yan, J. Knolle, C. A. Bridges, M. B. Stone, M. D. Lumsden, D. G. Mandrus, D. A. Tennant, R. Moessner, and S. E. Nagler, *Science* **356**, 1055 (2017).
- [30] S. M. Winter, A. A. Tsirlin, M. Daghofer, J. van den Brink, Y. Singh, P. Gegenwart, and R. Valentí, *J. Phys.: Condens. Matter* **29**, 493002 (2017).
- [31] M. Abramchuk, C. O. -Keskinbora, J. W. Krizan, K. R. Metz, D. C. Bell, and F. Tafti, *J. Am. Chem. Soc.* **139**, 15371 (2017).

- [32] Y. S. Choi, C. H. Lee, S. Lee, S. Yoon, W. J. Lee, J. Park, A. Ali, Y. Singh, J. C. Orain, G. Kim, J. S. Rhyee, W. T. Chen, F. Chou, and K. Y. Choi, *Phys. Rev. Lett.* **122**, 167202 (2019).
- [33] E. M. Kenney, C. U. Segre, W. L. D. -Hauret, O. I. Lebedev, M. Abramchuk, A. Berlie, S. P. Cottrell, G. Simutis, F. Bahrami, N. E. Mordvinova, G. Fabbris, J. L. McChesney, D. Haskel, X. Rocquefelte, M. J. Graf, and F. Tafti, *Phys. Rev. B* **100**, 094418 (2019).
- [34] S. K. Takahashi, J. Wang, A. Arsenault, T. Imai, M. Abramchuk, F. Tafti, and P. M. Singer, *Phys. Rev. X* **9**, 031047 (2019).
- [35] M. Ye, R. M. Fernandes, and N. B. Perkins, *Phys. Rev. Research* **2**, 033180 (2020).
- [36] M. Serbyn and P. A. Lee, *Phys. Rev. B* **87**, 174424 (2013).
- [37] A. Metavitsiadis and W. Brenig, *Phys. Rev. B* **101**, 035103 (2020).
- [38] K. Kitagawa, T. Takayama, Y. Matsumoto, A. Kato, R. Takano, Y. Kishimoto, S. Bette, R. Dinnebier, G. Jackeli, and H. Takagi, *Nature (London)* **554**, 341 (2018).
- [39] F. Bahrami, W. L. D. -Hauret, O. I. Lebedev, R. Movshovich, H. Y. Yang, D. Broido, X. Rocquefelte, and F. Tafti, *Phys. Rev. Lett.* **123**, 237203 (2019).
- [40] R. Yadav, R. Ray, M. S. Eldeeb, S. Nishimoto, L. Hozoi, and J. van den Brink, *Phys. Rev. Lett.* **121**, 197203 (2018).
- [41] Y. Li, S. M. Winter, and R. Valentí, *Phys. Rev. Lett.* **121**, 247202 (2018).
- [42] J. Knolle, R. Moessner, and N. B. Perkins, *Phys. Rev. Lett.* **122**, 047202 (2019).
- [43] S. Pei, L. L. Huang, G. Li, X. Chen, B. Xi, X. Wang, Y. Shi, D. Yu, C. Liu, L. Wang, F. Ye, M. Huang, and J. W. Mei, *Phys. Rev. B* **101**, 201101(R) (2020).
- [44] *Supplementary Information* (2020), (Link to be inserted later).
- [45] Y. Motome and J. Nasu, *J. Phys. Soc. Jpn.* **89**, 012002 (2020).
- [46] Y. S. Choi, R. Coldea, A. N. Kolmogorov, T. Lancaster, I. I. Mazin, S. J. Blundell, P. G. Radaelli, Y. Singh, P. Gegenwart, K. R. Choi, S. W. Cheong, P. J. Baker, C. Stock, and J. Taylor, *Phys. Rev. Lett.* **108**, 127204 (2012).
- [47] L. J. Sandilands, Y. Tian, K. W. Plumb, Y. J. Kim, and K. S. Burch, *Phys. Rev. Lett.* **114**, 147201 (2015).
- [48] D. Wulferding, Y. Choi, S. H. Do, C. H. Lee, P. Lemmens, C. Faugeras, Y. Gallais, and K. Y. Choi, *Nat. Comms.* **11**, 1603 (2020).

- [49] A. Glamazda, P. Lemmens, S. H. Do, Y. S. Kwon, and K. Y. Choi, *Phys. Rev. B* **95**, 174429 (2017).
- [50] J. Nasu, J. Knolle, D. L. Kovrizhin, Y. Motome, and R. Moessner, *Nat. Phys.* **12**, 912 (2016).
- [51] J. Menéndez and M. Cardona, *Phys. Rev. B* **29**, 2051 (1984).
- [52] P. G. Klemens, *Phys. Rev. B* **148**, 845 (1966).
- [53] L. Du, J. Tang, Y. Zhao, X. Li, R. Yang, X. Hu, X. Bai, X. Wang, K. Watanabe, T. Taniguchi, D. Shi, G. Yu, X. Bai, T. Hasan, G. Zhang, and Z. Sun, *Advanced Functional Materials* **29**, 1904734 (2019).
- [54] J. Nasu, M. Udagawa, and Y. Motome, *Phys. Rev. B* **92**, 115122 (2015).
- [55] S. J. Allen and H. J. Guggenheim, *Phys. Rev. B* **21**, 1807 (1968).
- [56] N. Suzuki and H. Kamimura, *J. Phys. Soc. Jpn.* **35**, 985 (1973).
- [57] B. Perreault, J. Knolle, N. B. Perkins, and F. J. Burnell, *Phys. Rev. B* **92**, 094439 (2015).
- [58] S. Bhattacharjee, S. Zherlitsyn, O. Chiatti, Sytcheva, J. Wosnitza, R. Moessner, M. E. Zhitomirsky, P. Lemmens, V. Tsurkan, and A. Loidl, *Phys. Rev. B* **83**, 184421 (2011).
- [59] J. Knolle, S. Bhattacharjee, and R. Moessner, *Phys. Rev. B* **97**, 134432 (2018).
- [60] Y. Kasahara, T. Ohnishi, Y. Mizukami, O. Tanaka, S. Ma, K. Sugii, N. Kurita, H. Tanaka, J. Nasu, Y. Motome, T. Shibauchi, and Y. Matsuda, *Nature* **559**, 227 (2018).

Figures

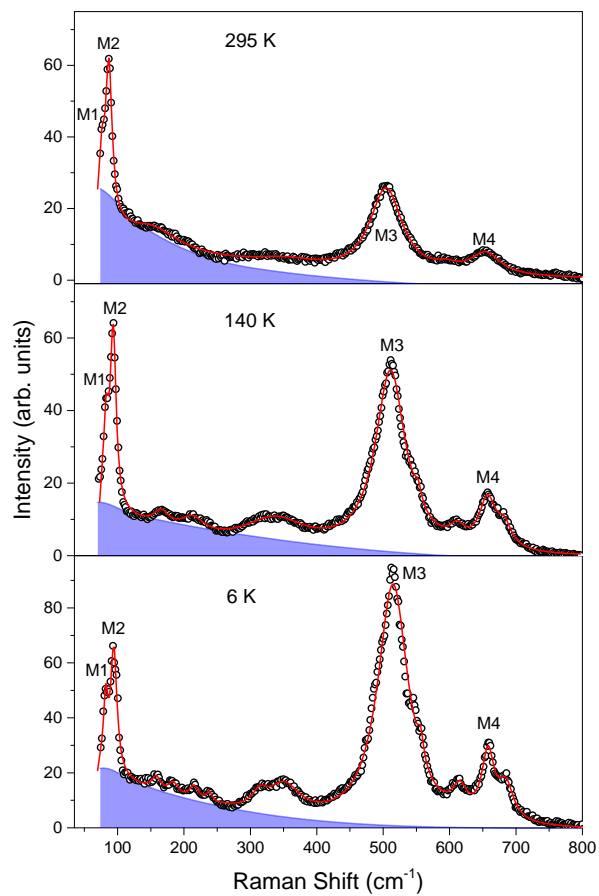


Figure 1: Fitted Raman spectra of Cu_2IrO_3 at three different temperatures in the spectral range $70 - 800 \text{ cm}^{-1}$. The shaded region represents the low-energy magnetic continuum. Data are shown by black circles. The solid red lines are the sum of individual phonon modes fitted with Lorentzian line shape.

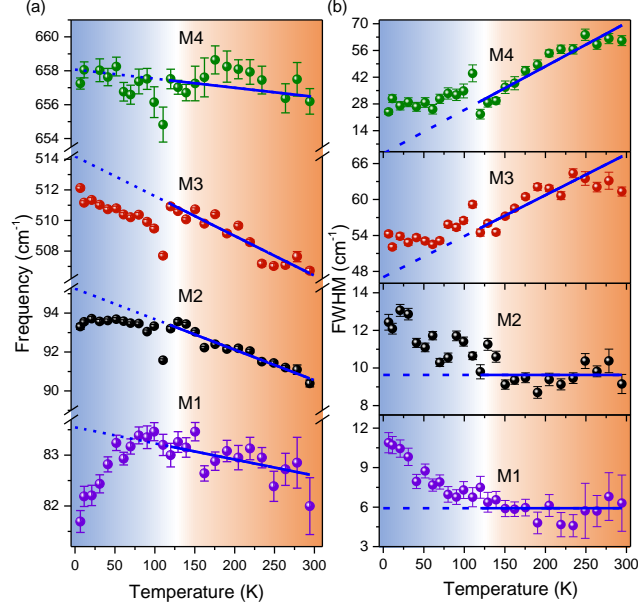


Figure 2: Temperature dependence of (a) phonon frequency and (b) FWHM. Blue solid lines are linear fits of the anharmonic model to phonon frequencies and FWHMs in the temperature range of 295 K - 120 K. Shaded regions demonstrate the boundary between the normal and the Kitaev paramagnetic states.

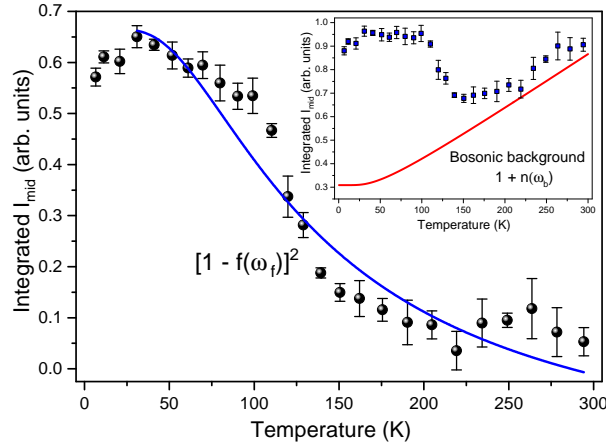


Figure 3: Symbols denote the magnetic contribution to integrated I_{mid} in the frequency range 90-230 cm^{-1} after subtracting the bosonic background (shown in the inset). The solid curve (blue online) represents fitting by the two-fermion scattering form $A+B(1-f)^2$, with $f = 1/(1+e^{\hbar\omega/k_B T})$ being the Fermi distribution function.

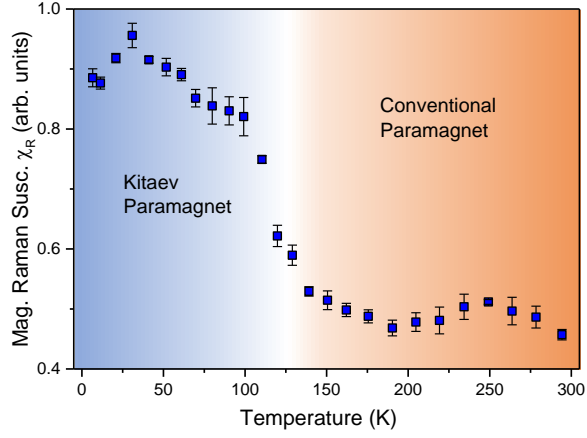


Figure 4: Magnetic Raman susceptibility as a function of temperature deduced from the Kramers-Kronig relation. The shaded regions mark the boundary between the conventional and Kitaev paramagnetic states.

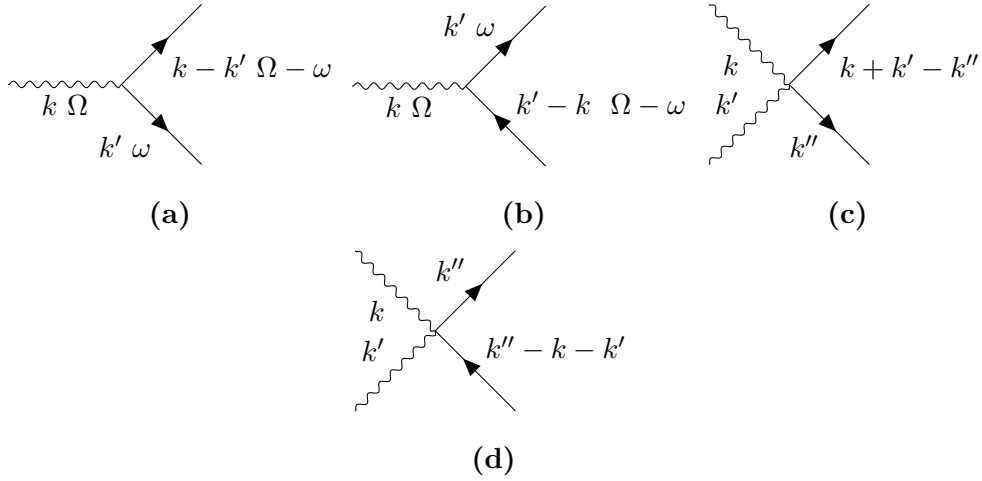


Figure 5: (a) and (b) denotes the contribution of Eq. 5 while (c) and (d) denotes the contribution of Eq. 6.

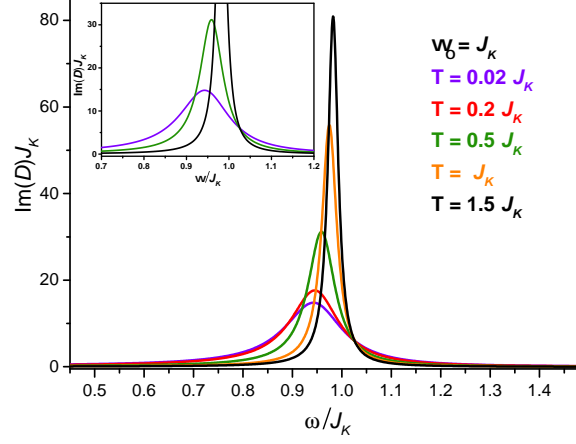


Figure 6: We plot the imaginary part of the phonon Green's function(D) with the frequency scaled w.r.t. the Kitaev coupling J_K . Different curves represent different temperatures. The spin-phonon coupling constants are taken as $\lambda = 0.13$ and $\chi = 0.2$.